# Buoyancy effects in stagnation-point flow of Maxwell fluid utilizing non-Fourier heat flux approach

Ammar Mushtaq[1]*, Meraj Mustafa[2], Tasawer Hayat[3,4], Ahmed Alsaedi[4]

1 Research Centre for Modeling and Simulation (RCMS), National University of Sciences and Technology (NUST), Islamabad, Pakistan, **2** School of Natural Sciences (SNS), National University of Sciences and Technology (NUST), Islamabad, Pakistan, **3** Department of Mathematics, Quaid-I-Azam University, Islamabad, Pakistan, **4** Department of Mathematics, Faculty of Science, King Abdulaziz University, Jeddah, Saudi Arabia

* ammar.mushtaq@yahoo.com

Competing interests: The authors have declared that no competing interests exist.
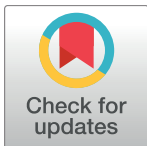
Abstract

Here we utilize a non-Fourier approach to model buoyancy aiding or opposing flow of Maxwell fluid in the region of stagnation-point towards a vertical stretchable surface. Flow field is permeated by uniform transverse magnetic field. Two different heating processes namely (i) prescribed surface temperature (PST) and (ii) constant wall temperature (CWT) are analyzed. Through suitable transformations, the similarity equations are formed which are treated numerically for a broad range of magnetic interaction parameter. The obtained solutions are compared with available articles under limiting situations and such comparisons appear convincing. The structure of boundary layer depends on a parameter measuring the ratio of free stream velocity to the stretching sheet velocity. The momentum transport via stretching boundary is opposed by both fluid relaxation time and magnetic interaction parameter. Thermal boundary layer expands as the effects of transverse magnetic field and thermal relaxation time are amplified. A reduction in heat penetration depth is anticipated for increasing values of thermal relaxation time. The variation in wall slope of temperature with increasing thermal relaxation time appears similar at any assigned value of Prandtl number. A comparative study of aiding and opposition flow situations is presented and deliberated.

Introduction

Non-Newtonian fluids such as polymers, lubricants, granular materials, biological fluids etc. abound in daily life and in industrial processes, for example, in chemical, food processing and oil industries. The phenomenon and constitutive relations of such liquids are significantly varied and complex than the traditional viscous fluid dynamics. Viscoelastic materials display both viscous and elastic behaviors when subjected to the shearing force. The elastic effect arises due to existence of macromolecules such as polymer molecules which have a high relaxation time compared to characteristic time. Stress relaxation time is an important characteristic of these liquids which is the time required for the decay of elastic effects. Some common

viscoelastic fluids are dough, yoghurt, cheese and gelled products. Viscoelastic fluid models of rate up involve one or more time derivatives and do not appear as explicit expression for stress tensor. In the past decade, Maxwell fluid model is frequently preferred by the researchers for the analysis of boundary layer problems. Maxwell fluid flow in the region of stagnation-point was analyzed by Sadeghy et al. [1] using spectral collocation point approach. They also made a comparison of results for Maxwell and second grade models. Consequences of buoyancy force on stagnation flow of Maxwell liquid near a deforming sheet were elucidated by Kumari and Nath [2]. Their results predicted that elastic effects have a retarding effect on fluid velocity. Hayat et al. [3] reported series approximations for electrically conducting flow of Maxwell fluid around a stagnation-point on a continuously deforming surface. Mukhopadhyay [4] modeled heat transfer effects in time dependent Maxwell fluid flow near a stretchable plate. Motsa et al. [5] made use of successive linearization procedure to treat the Maxwell fluid flow due to shrinking surface. A few important characteristics of boundary layer in Maxwell fluid were enlightened by Renardy and Wang [6]. Shateyi [7] provided a numerical treatment for magnetohydrodynamic (MHD) Maxwell fluid flow near a vertical surface considering the aspects of thermophoresis and chemical reaction. Bhattacharyya et al. [8] investigated multiple solutions for Maxwell fluid flow near a shrinking permeable boundary. Recently published material in this direction can be sought through refs. [9–17].

The phenomenon of heat transfer has abundant applications in numerous practical fields such as cooling towers, food processing, dispersion of temperature/moisture across groove fields, cooling of small electrical components such as microchips in computer processors, nanofluid flows, solar water cooling, enhancing performance efficiency of diesel engine oil and various others. Heat conduction model developed by Fourier [18] is of immense importance in modeling heat transfer in sundry situations. Foremost drawback of Fourier's approach is that it gives a paradoxical prediction that any initial disturbance would instantly alter the medium under observation. To overcome this drawback, a successful generalization to Fourier heat flux theory was devised by Cattaneo [19]. He used the concept of thermal relaxation time which refers to the time needed to achieve steady-state conduction in volume element when it is subjected to temperature differences. To preserve objectivity constraint, Christov [20] used the Oldroyd's upper-convected derivative in place of usual time derivative in Cattaneo's model to formulate energy equation. The Cattaneo-Christov approach was utilized by Straughan [21] to inspect convection in a horizontal layer of incompressible viscous fluid. Tibullo and Zampoli [22] proved uniqueness for incompressible flow problems based on Cattaneo-Christov model. Haddad [23] explored instabilities associated with the thermal transport in Brinkman layer with thermal relaxation effects. Han et al. [24] developed series approximations for Maxwell fluid flow near a deformable surface considering the aspects of Navier slip and Cattaneo-Christov conduction. Thermal relaxation effects in rotating viscoelastic fluid flow were analyzed by Mustafa [25]. He used both numerical and analytical techniques to treat the governing non-linear system. Khan et al. [26] reported simulations for viscoelastic fluid flow induced by an exponentially deforming surface considering a non-Fourier approach. Hayat et al. [27] investigated the onset of Cattaneo-Christov conduction for swirling flow of Jeffrey fluid past a porous surface. Mushtaq et al. [28] analyzed the Sakiadis flow in the framework of Cattaneo-Christov theory using two numerical approaches. Salahuddin et al. [29] examined the behavior of Lorentz force on Williamson fluid flow due to deforming sheet with thermal relaxation effects. Recently, a number of studies featuring Cattaneo-Christov model are published (see [30–34] and refs. there in.).

Stagnation flows are particularly important in predicting drag coefficient near stagnation region of bodies in high speed flows. Fluid flow around a stagnation-point towards a stretchable sheet has been a compelling research topic because it is met in many metal working and polymer

extrusion processes. The pioneering study of Heimenz [35] concerning the plane stagnation-point flow has led to may subsequent research activities. For example, Mahapatra et al. [36] modeled stagnation-point flow of conducting power-law fluid bounded by a stretchable surface. In this study, numerical calculations were made for full range of magnetic interaction parameter. Consequence of wall permeability on the stagnation-point flow near a shrinking sheet was discussed by Bhattacharyya et al. [37]. In another study, Bhattacharyya et al. [38] provided numerical analysis for MHD fluid flow around a stagnation-point with chemically reactive solute. Bhattacharyya [39] presented dual solutions for thermal transport in stagnation-point flow considering variable heat flux at the boundary. Also, Bhattacharyya [40] examined solute transfer in stagnation-point flow caused by shrinking surface with diffusive mass fluid conditions.

Inspired by the aforementioned studies, we intend to investigate the onset of mixed convection in Maxwell fluid flow due to heated or cooled vertical surface utilizing Cattaneo-Christov heat flux model. Flow field is influenced by vertical magnetic field of uniform strength. Studies presented through [41–47] demonstrate the fact that buoyancy forces resulting from the heating of the deformable surfaces are useful in terms of drag reduction and heat transfer intensification. Unlike previous studies [2], [3], [4] and [9], we consider the correct form of body force terms representing magnetic and gravitational potentials. Conventional transformations are adopted to extract local similarity equations which are treated via efficient shooting approach, the details of which can be found in [28]. For validation purpose, the results are compared with published papers in special cases and found in complete agreement. Alternative computational approaches for similar kind of boundary layer problems can be seen through [48–51] and studies there in. The impacts of important parameters on the momentum and energy transport are the main concerns of this investigation. The rest of the paper is arranged in the following manner. Mathematical formulation is covered in the next section. Section 3 gives a detailed description of the employed numerical treatment. In section 4, physical description to the behavior of emerging parameters is assigned graphically. Finally, the conclusion section highlighting major results is presented.

Problem formulation

Consider a laminar viscoelastic fluid flow adjacent to a vertical elastic sheet with u and v denoting velocity components along $x-$ and $y-$ directions in which the coordinate x extends along the sheet and y is normal to it. Let us assume that the surface stretches in $x-$ direction with velocity $u_w(x) = ax$ and $u_e(x) = cx$ denotes the velocity of external flow where a and c are positive constants. The buoyancy force resulting due to density differences aids or opposes the external flow when it is directed towards or opposite to the external stream. The conducting Maxwell fluid is exposed to transverse magnetic field of strength B_0 (see Fig 1). Under low magnetic Reynolds number, induced magnetic field can be ignored in comparison with the applied magnetic field. There is no electric field. Thus if σ denotes the fluid electrical conductivity, the components of Lorentz force vector become $(-\sigma B_0^2 u, -\sigma B_0^2 v, 0)$. The function $T_w(x) = T_\infty + bx$ prescribes the wall temperature in which b is a constant and T_∞ represents the temperature of quiescent fluid. Utilizing the Oberback-Boussinesq approximation, equations representing Maxwell fluid motion with heat transfer are given below (see refs. [14] and [20]):

$$u_x + v_y = 0 \tag{1}$$

$$uu_x + vu_y + \lambda_1(u^2 u_{xx} + v^2 u_{yy} + 2uv u_{xy}) = u_e(u_e)_x + vu_{yy} - \frac{\sigma}{\rho}B_0^2(u - u_e + \lambda_1 v u_y)$$

$$+g\beta_T[(T - T_\infty) + \lambda_1\{uT_x + vT_y - u_x(T - T_\infty)\}], \tag{2}$$
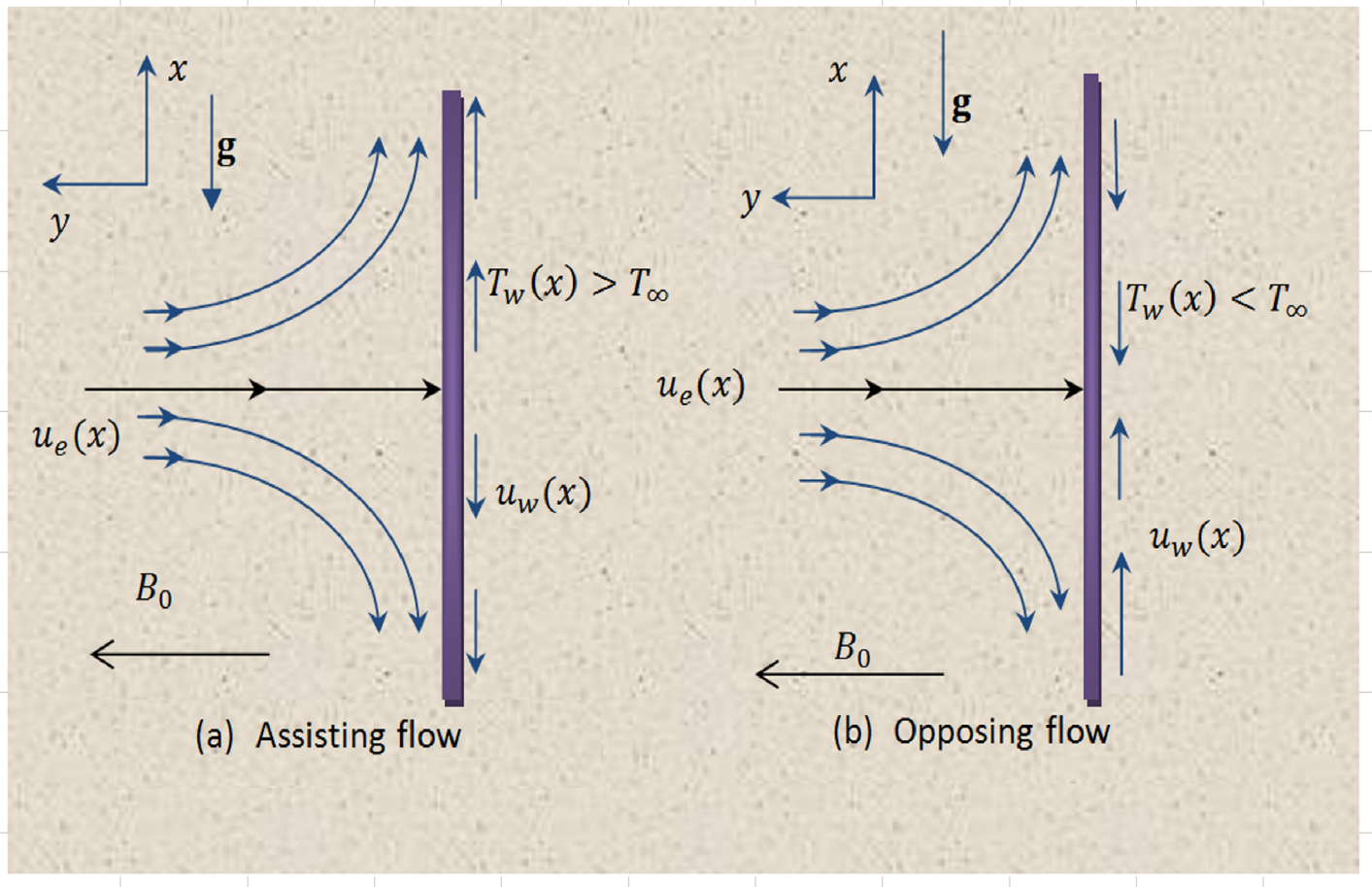
Fig 1. Physical model and coordinate system.

$$\rho C_p(uT_x + vT_y) = -\nabla \cdot \mathbf{q}, \tag{3}$$

where λ_1 stands for fluid relaxation time, v denotes the kinematic viscosity, ρ is the fluid density, β_T stands for the coefficient of thermal expansion, C_p denotes the specific heat capacity and $\mathbf{q}$ the heat flux vector. Using Cattaneo-Christov theory, the heat flux $\mathbf{q}$ obeys the following relation [20, 24]:

$$\mathbf{q} + \lambda_2(\mathbf{q}_t + \mathbf{V} \cdot \nabla \mathbf{q} - \mathbf{q} \cdot \nabla \mathbf{V} + (\nabla \cdot \mathbf{V})\mathbf{q}) = -k\nabla T, \tag{4}$$

in which k denotes the fluid thermal conductivity and λ_2 stands for thermal relaxation time. Taking divergence of Eq (4) and then utilizing Eq (3), one arrives at the following equation:

$$uT_x + vT_y + \lambda_2\{u^2T_{xx} + v^2T_{yy} + 2uvT_{xy} + (uu_x + vu_y)T_x + (uv_x + vv_y)T_y\} = \alpha T_{yy}. \tag{5}$$

For detailed derivation of Eq (5), the readers are referred to the article by Christov [20]. The boundary conditions assume the following forms:

$$u(x,0) = u_w(x) = ax, \quad T(x,0) = \begin{cases} T_\infty + bx \ \ (\text{PST}) \\ T_w \ \ (\text{CWT}) \end{cases}, \tag{6}$$

$$v(x,0) = 0, \tag{7}$$

$$u \to u_e(x) = cx, \ v \to v_e(y) = -cy \ \text{ as } \ y \to \infty, \tag{8}$$

$$T \to T_\infty \ \text{ as } y \to \infty. \tag{9}$$

Conditions given in (6) indicates no-slip at the wall, condition (7) represent impermeability at the boundary, condition (8) indicates that viscous effects vanish at far distance from the surface and condition (9) signifies no temperature variation far from the boundary.

Defining the non-dimensional horizontal distance $\zeta = y(a/v)^{1/2}$, we seek the similarity solutions of (1), (2) and (5) of the following forms:

$$u = axF'(\zeta), \ v = -(va)^{1/2}F(\zeta), \ \theta(\zeta) = (T - T_\infty)/(T_w - T_\infty). \tag{10}$$

Eq (1) is satisfied by transformations (10), while Eqs (2), (5) and (6)–(9) convert into the following ordinary differential equations:

$$F''' + (1 + M\beta)FF'' - F'^2 + \beta(2FF'F'' - F^2F''') - MF'$$
$$+ \lambda(\theta - \beta F\theta') + M\frac{c}{a} + \frac{c^2}{a^2} = 0, \tag{11}$$

$$\frac{1}{\text{Pr}}\theta'' + F\theta' - F'\theta - \gamma(F^2\theta'' + FF''\theta + F'^2\theta - FF'\theta') = 0 \quad (\text{PST}), \tag{12}$$

$$\frac{1}{\text{Pr}}\theta'' + F\theta' - \gamma(F^2\theta'' - FF'\theta') = 0 \quad (\text{CWT}), \tag{13}$$

$$F = 0, \ F' = 1, \ \theta = 1 \quad \text{at} \quad \zeta = 0,$$
$$F' \to \frac{c}{a}, \ \theta \to 0 \quad \text{as} \quad \zeta \to \infty. \tag{14}$$

In Eq (8), $\lambda = Gr_x/Re_x^2$ is the mixed convection parameter (also called Richardson number) in which $Gr_x = g\beta_T(T_w - T_\infty)x^3/v^2$ denotes the local Grashof number and $Re_x = u_wx/v$ is the local Reynolds number. For positive values of λ we have $T_w > T_\infty$ in the upper half (where $x > 0$) while $T_w < T_\infty$ in the lower half (where $x < 0$). In this situation, buoyancy force acts in the same direction as that of free stream velocity in both upper and lower halves, thereby assisting the fluid flow. For negative λ, buoyancy force is directed opposite to the external stream in both upper and lower halves. The other parameters appearing in (11) and (12)-(13) are given below:

$$M = \sigma B_0^2/\rho a, \ \text{Pr} = v/\alpha, \ \beta = \lambda_1 a, \ \gamma = \lambda_2 a, \tag{15}$$

where M denotes the magnetic interaction parameter, Pr denotes the Prandtl number, β stands for fluid relaxation time and γ for thermal relaxation time. A list of all symbols is shown in

Table 1. Note that Eqs ([11](#), [12](#) and[13](#)) reduce to the viscous fluid case when $\beta = 0$. Also, the analysis for usual Fourier law can be recovered by selecting $\gamma = 0$.

Numerical procedure

Here we discuss the numerical treatment of governing Eqs. ([11](#)) and ([12](#)) using shooting method coupled with Runge-Kutta method of fifth-order and the Newton's method. Making use of the substitutions $y_1 = F, y_2 = F', y_3 = F'', y_4 = \theta, y_5 = \theta'$, an initial value problem consisting of five first order ordinary differential equations is obtained:

$$y_1' = y_2; \quad y_1(0) = 0$$

$$y_2' = y_3; \quad y_2(0) = 1$$

$$y_3' = \frac{y_2^2 - (1 + M\beta)y_1 y_3 - 2\beta y_1 y_2 y_3 - \lambda(y_4 - \beta y_1 y_5) + M(y_2 - c/a) - (c/a)^2}{1 - \beta y_1^2}; \quad y_3(0) = s_1 \quad (16)$$

$$y_4' = y_5; \quad y_4(0) = 1$$

$$y_5' = \frac{\Pr\{y_2 y_4 - y_1 y_5 + \gamma(y_1 y_3 y_4 + y_2^2 y_4 - y_1 y_2 y_5)\}}{1 - \Pr\gamma y_1^2}; \quad y_5(0) = s_2 \,.$$

We replace infinity (∞) by a number, say ζ_∞, which is initially taken as low as 2 and then proceed with the numerical integration of system (16) by assigning suitable guesses for the missing slopes $s_1 = F''(0)$ and $s_2 = \theta'(0)$. It means that a solution to the system (16) will depend on similarity variable ζ and the missing slopes s_1 and s_2. Here the mesh size $h = 0.01$ is considered in numerical integration. Thus conditions for F' and θ at infinity can be expressed as $y_2(\zeta_\infty, s_1, s_2) - (c/a) = 0$ and $y_4(\zeta_\infty, s_1, s_2) = 0$ respectively. These algebraic equations are solved for s_1 and s_2 by Newton's method. Solutions for s_1 and s_2 are employed in (16) and the system is integrated at a higher ζ_∞, say $\zeta_\infty = 4$. We repeat this process for different ζ_∞(say $\zeta_\infty = 5, 6, 7$ etc.) until the solutions for s_1 and s_2 become independent of ζ_∞. In Newton's method, computer code is designed to perform maximum 30 iterations. Our computations have shown

Table 1. List of symbols.

x,y Cartesian coordinates (m)	Re_x local Reynolds number
(u,v) velocity components along x-and y-directions respectively (ms^{-1})	*Greek symbols*
(u_e, v_e) external flow velocity components in (ms^{-1})	ζ similarity variable
u_w velocity of stretching sheet (ms^{-1})	σ electrical conductivity (s.m^{-1})
a,c positive constants (s^{-1})	ρ fluid density (kg.m^{-3})
B_0 magnetic field strength (Nm^{-1}A^{-1})	ν kinematic viscosity (m^{2}s^{-1})
M magnetic interaction parameter	α thermal diffusivity (m^{2}s^{-1})
g gravitational acceleration (ms^{-2})	λ Richardson number
T fluid temperature (K)	λ_1 fluid relaxation time (s)
T_w wall temperature (K)	λ_1 heat flux relaxation time (s)
T_∞ ambient fluid temperature (K)	γ dimensionless thermal relaxation time
C_p specific heat (Jkg^{-1}K^{-1})	β dimensionless fluid relaxation time
q heat flux(Wm^{-2})	β_T coefficient of thermal expansion (K^{-1})
k thermal conductivity (Wm^{-1}K^{-1})	θ dimensionless temperature
F dimensionless stream function	*Subscripts*
Pr Prandtl number	w condition at the wall
Gr_x local Grashof number	∞ condition at infinity

that such number of iterations is sufficient to fulfill the desired tolerance of 10^{-7} in all the considered cases.

Numerical results and discussion

We modeled the aiding or opposing mixed convection viscoelastic fluid flow adjacent to a heated vertical surface utilizing the novel Cattaneo-Christov model. A convenient shooting technique is implemented to compute the governing similarity equations. In Table 2, the values of $F''(0)$ are compared with those of Mahapatra et al. [36] for broad range of magnetic interaction parameter M in Newtonian limit ($\beta = 0$). Present numerical results are in complete agreement with [36] for all reported values of M. For a further check, we made comparison of values of $F''(0)$ with Mustafa et al. [34], Abel et al. [52] and Megahed [53] for the forced convection flow situation ($\lambda = c/a = 0$). Again we witness a very good agreement for all chosen values of Deborah number β (see Table 3). The values of wall temperature slope $\theta'(0)$ for various parameter values are listed in Table 4. It is indicated in [48] that Prandtl number for non-Newtonian fluids is usually large. Hence numerical calculations are made at Pr = 10 and Pr = 25. An increasing trend in $|\theta'(0)|$ is found for increasing values of dimensionless thermal relaxation time γ. CPU time for the numerical values computed in Table 4 is mentioned against each simulation.

For fixed values of mixed convection parameter λ and Deborah number β, the curves of $F'(\zeta)$ representing x−component of velocity are portrayed in Fig 2 for different values of magnetic interaction parameter M and velocity ratio (c/a). Velocity parallel to the surface decreases with increasing M for (c/a) < 1 but increases with increases M for (c/a) > 1. For any value of velocity ratio (c/a) we witness a decreasing trend in boundary layer thickness for increasing values of M. It is the consequence of the fact that magnetic field sets up a Lorentz force in transverse direction which retards the momentum transport phenomenon.

Fig 3 shows the velocity curves $F'(\zeta)$ for varying velocity ratio (c/a) in both assisting and opposing flow regimes. An increase in (c/a) can be realized by increasing free stream velocity

Table 2. Comparison of velocity gradient $|F''(0)|$ with that of Mahapatra et al. [36] when $\beta = \lambda = 0$.

M	(c/a) = 2		(c/a) = 0.2	
	[36]	Present	[36]	Present
0.0	2.0175	2.01750	0.9181	0.91811
0.5	2.1363	2.13632	1.0768	1.07682
1.0	2.2491	2.24910	1.2156	1.21562
1.5	2.3567	2.35667	1.3404	1.34038
2.0	2.4597	2.45967	1.4546	1.45460
3.0	2.6540	2.65398	1.6569	1.65979
5.0	3.0058	3.00578	2.0085	2.00847
10	3.7447	3.74472	2.6894	2.68944
20	4.9004	4.90037	3.6922	3.69223
40	6.6339	6.63381	5.1412	5.14123
60	8.0002	8.00032	6.2635	6.26356
80	9.1642	9.16537	7.2136	7.21333
100	10.1934	10.19819	8.052	8.05184
200	14.2825	14.28291	11.3491	11.35042
300	17.4127	17.43563	13.8537	13.88640
500	22.4499	22.44996	17.8617	17.91178
1000	31.6858	31.68596	25.1163	25.31466

Table 3. Comparison with wall velocity gradient −$F''(0)$ obtained by Mustafa et al. [34], Abel et al. [52] and Megahed [53] for different values of β when λ = (c/a) = 0.

β	Mustafa et al. [34]	Abel et al. [52]	Megahed [53]		Present	
				$\zeta_\infty = 2$	$\zeta_\infty = 5$	$\zeta_\infty = 10$
0	1.000000	0.999962	0.999978	1.000000	1.000000	1.000000
0.2	1.051890	1.051948	1.051945	1.051921	1.051890	1.051890
0.4	1.101903	1.101850	1.101848	1.101789	1.101903	1.101903
0.6	1.150137	1.150163	1.150160	1.150168	1.150137	1.150137
0.8	1.196711	1.196692	1.196690	1.196682	1.196711	1.196711
1.2	1.285363	1.285257	1.285253	1.285324	1.285363	1.285363
1.6	1.368758	1.368641	1.368641	1.368715	1.368758	1.368758
2.0	1.447651	1.447617	1.447616	1.447639	1.447651	1.447651

https://doi.org/10.1371/journal.pone.0192685.t003

while maintaining the same stretching rate (or by decreasing the stretching rate while keeping the free stream velocity fixed). We observe that $F'(\zeta)$ is proportional to (c/a) whereas boundary layer thickness decreases with increasing (c/a). Physically an increment in (c/a) implies a reduction in the straining motion near the surface which in turn reduces the thickness of hydrodynamic boundary layer.

In Fig 4, we present the change in velocity profile $F'(\zeta)$ with the variation in Deborah number β. In assisting or opposing flow regime, fluid flow in vertical direction accelerates when β becomes large for (c/a) > 1 while opposite effect is observed for (c/a) < 1. Notably, a decreasing trend in boundary layer thickness is found for increasing β and such outcome persists for

Table 4. Computational results of −$\theta'(0)$ for varying values of γ, (c/a) and β with Pr = 10 and M = 5.

γ	(c/a)	β	Pr = 10		Pr = 25	
			Assisting Flow λ = 1	Opposing Flow λ = −1	Assisting Flow λ = 1	Opposing Flow λ = −1
0.2	0.3	0.2	3.978577 (32.270 sec)	3.910338 (35.197 sec)	6.551186 (60.005 sec)	6.50699 (63.613 sec)
0.4			4.354726 (13.898 sec)	4.284905 (23.047 sec)	7.128445 (36.352 sec)	7.086098 (59.329 sec)
0.6			4.693003 (45.715 sec)	4.613185 (57.069 sec)	7.623144 (13.964 sec)	7.555093 (13.637 sec)
0.8			4.959215 (16.371 sec)	4.932692 (27.048 sec)	7.947736 (8.273 sec)	7.915262 (8.407 sec)
0	0	0.2	3.357325 (2.481 sec)	3.270179 (2.524 sec)	5.659030 (2.871 sec)	5.609332 (2.877 sec)
	0.4		3.641242 (2.737 sec)	3.588133 (2.606 sec)	5.921715 (2.925 sec)	5.883671 (2.921 sec)
	0.6		3.761313 (2.837 sec)	3.715780 (2.651 sec)	6.044662 (2.961 sec)	6.010370 (2.971 sec)
	1.2		4.084024 (2.760 sec)	4.051657 (2.565 sec)	6.395400 (3.526 sec)	6.368817 (2.060 sec)
0.2	0.3	0	4.002944 (38.038 sec)	3.945292 (35.149 sec)	6.570579 (67.316 sec)	6.534230 (60.089 sec)
		0.2	3.978577 (32.270 sec)	3.910338 (35.197 sec)	6.551186 (60.005 sec)	6.50699 (63.613 sec)
		0.4	3.954021 (32.740 sec)	3.875656 (28.188 sec)	6.530987 (67.533 sec)	6.478746 (64.059 sec)
		0.8	3.905982 (27.809 sec)	3.808797 (23.860 sec)	6.488601 (63.526 sec)	6.420623 (61.060 sec)

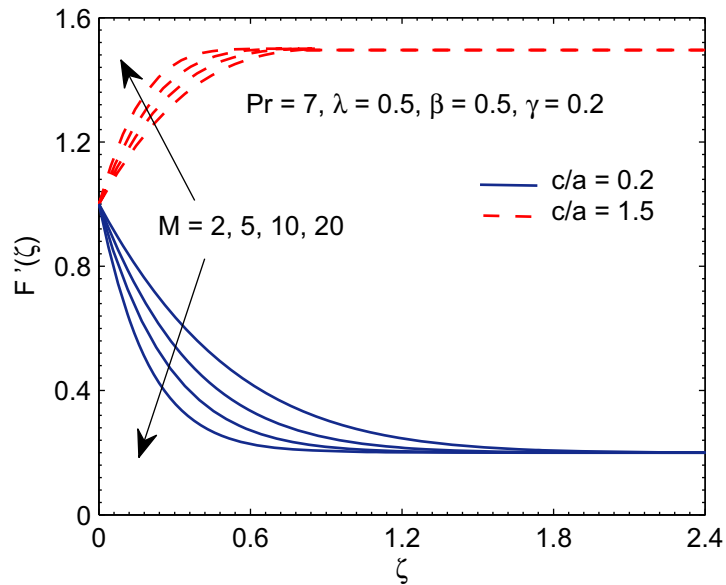https://doi.org/10.1371/journal.pone.0192685.t004

Fig 2. Curves of F' for various values of magnetic interaction parameter M.

any assigned value of (c/a). This is explained as follows. At low Deborah number, stress relaxation is fast in comparison to the observation time scale, and hence fluid has solid-like response to the shearing force. At higher Deborah number, the fluid response resembles closely to that of an elastic solid substance. In this situation, the boundary layer thickness does not grow as fast as for smaller Deborah number.
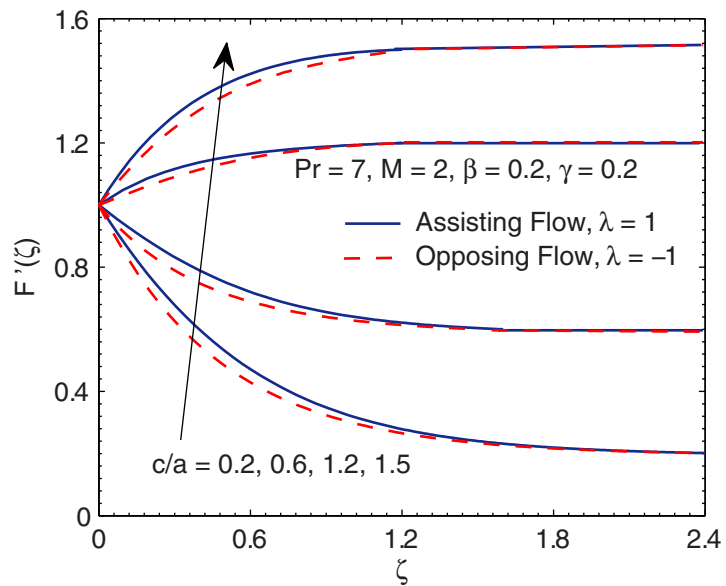
Fig 3. Curves of F' for various values of velocity ratio parameter (c/a).
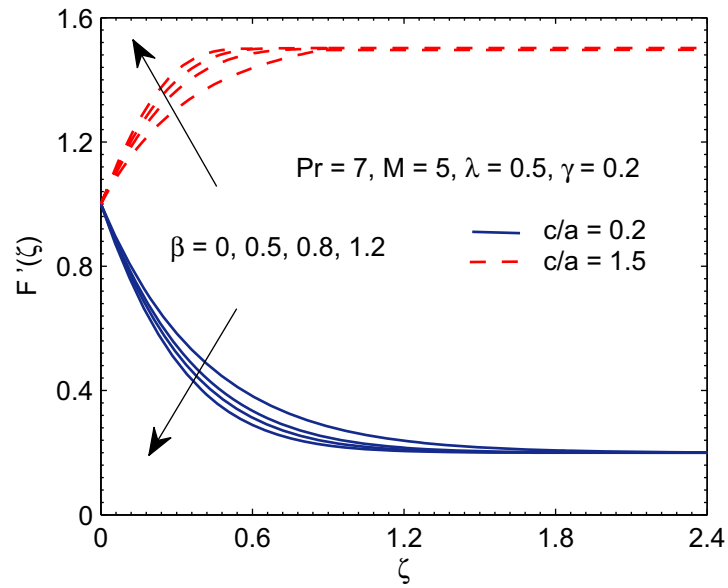
Fig 4. Curves of F' for various values of Deborah number β.

Fig 5 depicts the change in velocity curves by varying mixed convection parameter λ. It is observed that velocity in $x-$direction has direct relationship with λ. The result is in accordance with those reported by earlier studies (for instance see Kumari and Nath [9], Ali et al. [44] etc.). This trend follows from the fact that positive λ acts as favorable pressure gradient which accelerates the fluid flow in the boundary layer.
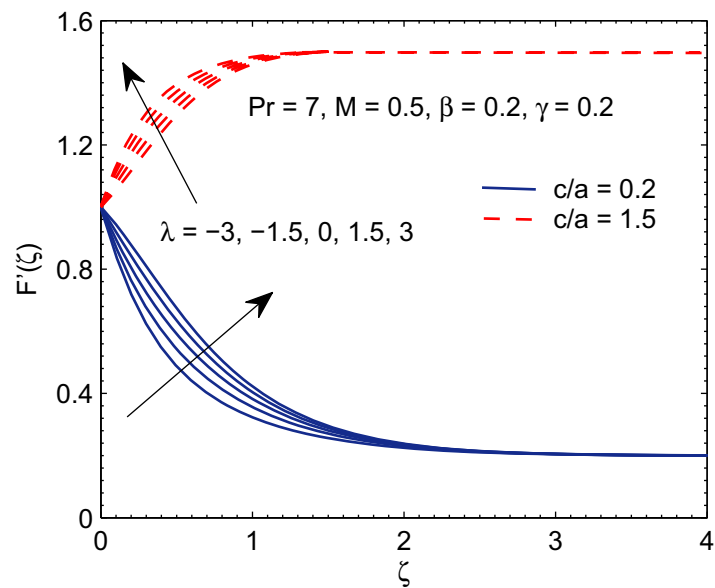
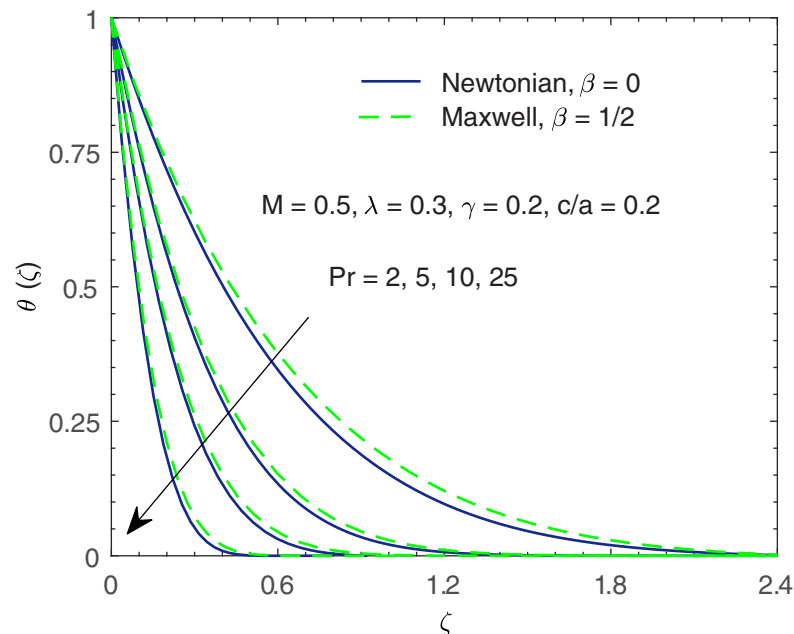**Fig 5. Profiles of F' for different values of mixed convection parameter γ.**

Fig 6. Profiles of θ for various values of Prandtl number Pr.

Fig 6 shows the temperature curves, represented by $\theta(\zeta)$, with the change in Prandtl number Pr. Prandtl number gives the ratio of momentum diffusion coefficient to thermal diffusion coefficient. In some manufacturing processes, the Prandtl number can be used to adjust the cooling rate. As emphasized in [53], non-Newtonian fluids have relatively high Prandtl number. At higher Prandtl number, heat convection is dominant over pure conduction. In other words, heat transfer rate at the stretching boundary grows with increasing Pr. The larger heat transfer rate implies shorter penetration depth due to which temperature decreases.

Temperature curves for varying magnetic interaction parameter M are displayed in Fig 7. Fluid temperature in the boundary layer rises for growing magnetic field strength. This is because less hot fluid is carried away from the surface due to reduction in velocity with increasing M which in turn yields smaller wall temperature gradient.

In Fig 8, the profiles of temperature θ are plotted by varying thermal relaxation time γ. We found that temperature $\theta(\zeta)$ has a decreasing behavior for increasing thermal relaxation time γ. It implies that heat penetration into the fluid reduces as relaxation duration for heat flux increases.

The impact of velocity ratio parameter (c/a) on temperature profile θ is depicted through Fig 9. In Fig 3, we observed that fluid flow accelerates in vertical direction with an increment in (c/a) for $\lambda > 0$. This eventually intensifies the horizontal flow of cold fluid at the ambient towards hot surface which in turn decreases temperature distribution.

Having tested the accuracy of method, we now intend to give physical description to the role of involved parameters on the solution profiles. When $(c/a) = 1$, the fluid and stretching boundary have same velocities, which results in no-frictional effect at the fluid-solid interface, that is, $F''(0) = 0$. When $(c/a) > 1$, the free stream moves faster than the stretching surface, which implies that fluid applies drag on the boundary due to which $F''(0) > 0$ (see Fig 10). However when $(c/a) < 1$, the stretching surface moves faster than the external free stream and hence it applies drag on the fluid. In this case $F''(0)$ has a negative sign. In Fig 10, we display
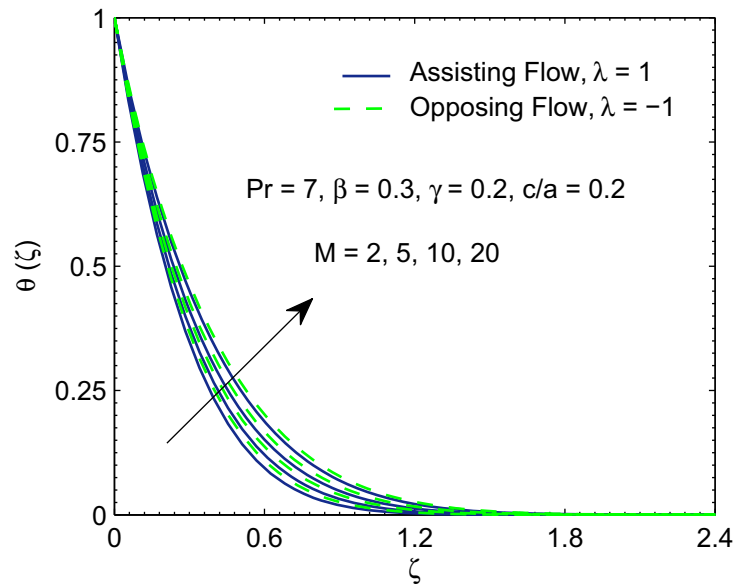
Fig 7. Profiles of θ for various values of magnetic interaction parameter M.

https://doi.org/10.1371/journal.pone.0192685.g007

the profile of $F''(0)$ versus magnetic interaction parameter M for a variety of velocity ratio parameters. Magnitude of $F''(0)$ continues to enhance as magnetic interaction parameter becomes large. Physically, the reduction in boundary layer thickness due to enhancement in M implies an elevation in wall slope of velocity field F'. In Fig 11, we give a comparative study of Fourier and Cattaneo-Christov models. Although, qualitatively similar behavior of Prandtl number Pr on $\theta'(0)$ is found in both models but the variation in $\theta'(0)$ with increasing Pr becomes prominent as thermal relaxation time become large. Solutions for non-similar partial
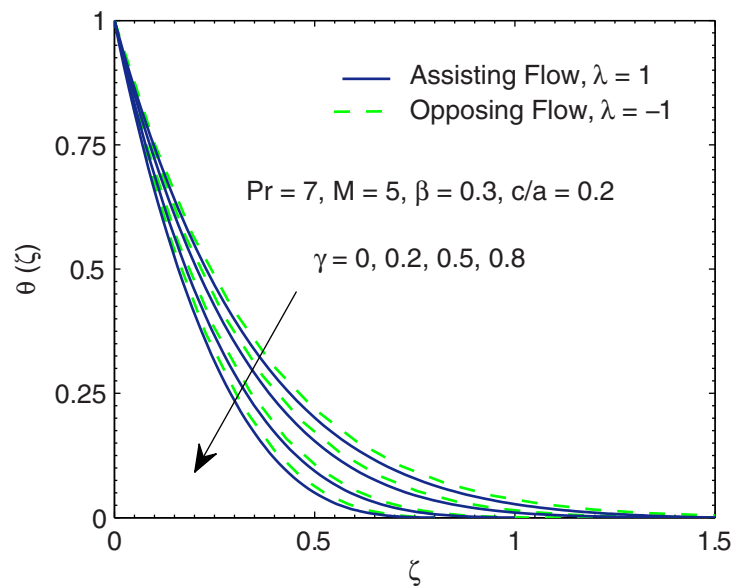

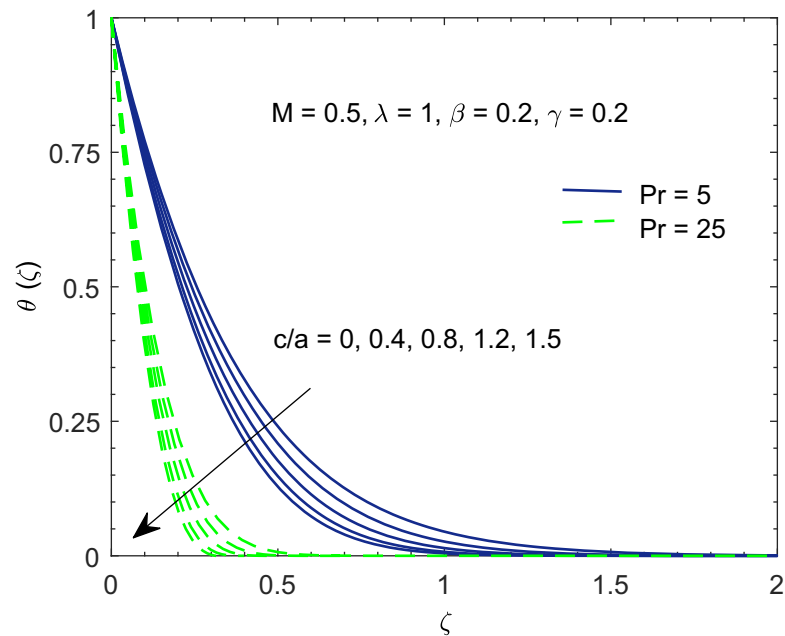**Fig 8. Curves of θ for various values of thermal relaxation time γ.**

https://doi.org/10.1371/journal.pone.0192685.g008

Fig 9. Profiles of θ for various values of velocity ratio parameter (c/a).

differential equations have been presented in terms of stream function $\phi(x,y)$ and temperature $T(x,y)$ in Figs 12 and 13. The profiles of temperature θ for constant and variable wall temperature (Similar and Nonsimilar solutions) with variation of Pr are plotted in Fig 14.

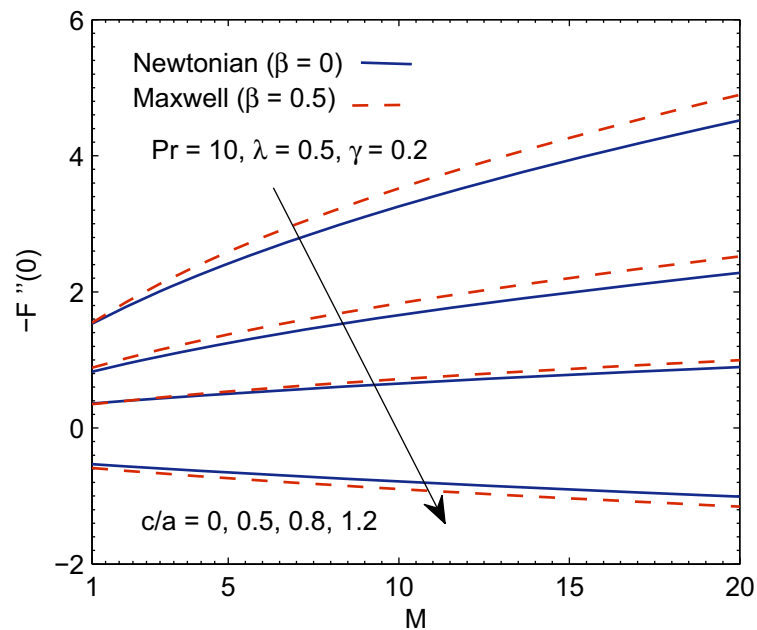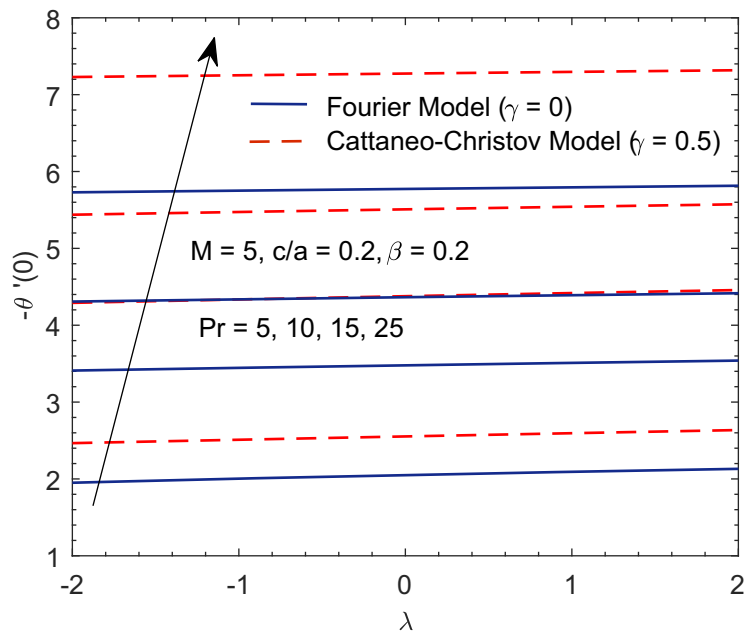**Fig 10. Profiles of $-F''(0)$ for various parametric values.**

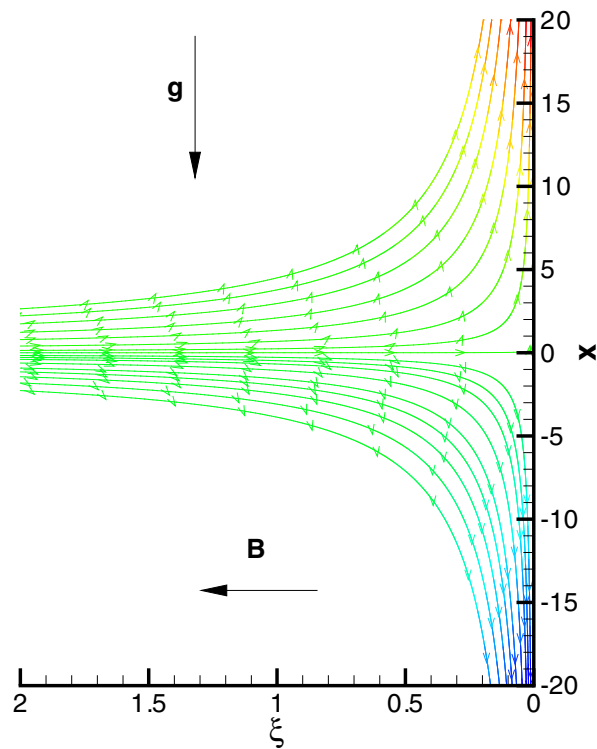**Fig 11. Profiles of $-\theta'(0)$ for various parametric values.**

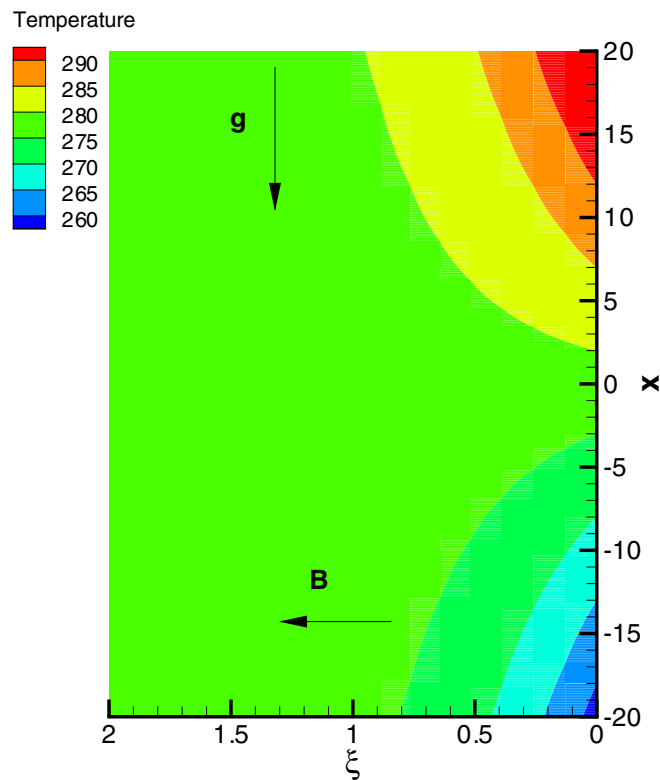**Fig 12. Plots of stream function when $c/a = 0.2, \beta = 0.2, M = \lambda = 1.$**

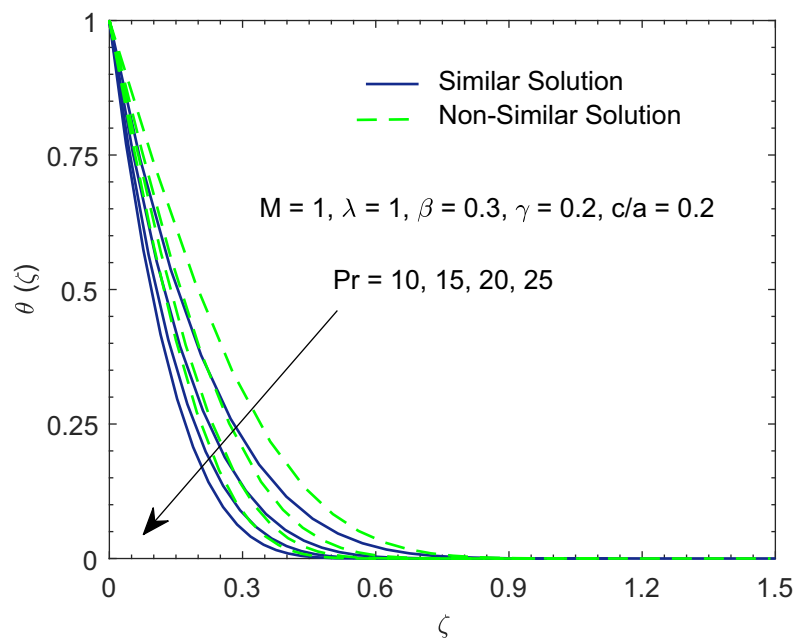**Fig 13. Isotherms for $T_\infty = 278K$, Pr = 10, $\gamma = 0.2$, $\lambda = 1$.**

Fig 14. Profiles of θ for various values of Prandtl number Pr in both nonsimilar and Similar cases.

Summary of the results

Cattaneo-Christov heat conduction for mixed convection Maxwell fluid flow adjacent to a heated or cooled vertical surface is investigated here. Flow fields are influenced by vertical magnetic field. Accurate numerical results are presented for broad range of magnetic interaction parameter ($0 \leq M \leq 1000$) and moderate values of viscoelastic fluid parameter β. Following conclusions are drawn on the basis of current analysis:

- Transverse magnetic field opposes the momentum transport by deformingsheet while fluid temperature rises for intensifying magnetic field strength.

- A reduction in momentum boundary layer thickness is anticipated for growing fluid relaxation time.

- Fluid flow in vertical direction decelerates with increasing magnetic interaction parameter M and viscoelastic parameter β for $(c/a) < 1$. However opposite effect is found in the case where $(c/a) > 1$.

- For any choice of velocity ratio (c/a), vertical velocity increases/decreases with increasing strength of buoyancy assisting/opposing force.

- Fluid temperature falls inside the boundary layer as relaxation time for heat flux enlarges.

- As velocity ratio parameter (c/a) enlarges, this accelerates the flow of cold fluid at the ambient towards the plate. Consequently, fluid temperature inside the boundary layer falls for increasing velocity ratio parameter (c/a).

- Fluid temperature inside the boundary layer increases/decreases as the strength of buoyancy assisting/opposing force increases.

- Present computations are consistent with those of available articles [34], [36], [52] and [53] in limiting situations.

Appendix

Here we will present the details concerning the derivation of Eq (2).

Relevant equation governing the two-dimensional flow of incompressible Maxwell fluid along a vertical surface with transverse magnetic field can be expressed as follows:

$$\rho \frac{d\mathbf{V}}{dt} = -\nabla p + \nabla \cdot \mathbf{S} + \rho \mathbf{g} \beta_T (T - T_\infty) + \mathbf{J} \times \mathbf{B}, \qquad (17)$$

in which $\mathbf{V} = [u(x,y), v(x,y), 0]$ denotes the velocity vector, $\mathbf{g} = [0, g, 0]$ is gravitational acceleration, $\mathbf{J} = \sigma(\mathbf{E} + \mathbf{V} \times \mathbf{B})$ denotes the current density in which $\mathbf{B} = [0, B_0, 0]$ is the applied magnetic field and $\mathbf{E}$ denotes the electric field intensity, $d/dt \equiv \partial/\partial t + (\mathbf{V} \cdot \nabla)\mathbf{V}$ is the material time derivative and $\mathbf{S}$ is the extra stress tensor which obeys the following relation:

$$\left(1 + \lambda_1 \frac{D}{Dt}\right)\mathbf{S} = \mu \mathbf{A}_1. \qquad (18)$$

Here λ_1 is the fluid relaxation time, $\mathbf{A_1} = (\nabla \mathbf{V}) + (\nabla \mathbf{V})^t$ is the first Rivlin-Ericksen tensor and D/Dt the convected time derivative. For any vector $\mathbf{A}$, we have:

$$\frac{D\mathbf{A}}{Dt} = \frac{\partial \mathbf{A}}{\partial t} + (\mathbf{V} \cdot \nabla)\mathbf{A} - (\nabla \mathbf{V}) \cdot \mathbf{A}, \qquad (19)$$

In order to eliminate **S**, let us assign the operator $\left(1 + \lambda_1 \frac{D}{Dt}\right)$ to Eq (17). We obtain the following:

$$\rho\left(1 + \lambda_1 \frac{D}{Dt}\right)\left[\frac{d\mathbf{V}}{dt} - \rho\mathbf{g}\beta_T(T - T_\infty) - \mathbf{J} \times \mathbf{B}\right] = -\left(1 + \lambda_1 \frac{D}{Dt}\right)\nabla p + \mu(\nabla.\mathbf{A_1}), \qquad (20)$$

Making use of definition (19) and boundary layer approximations, x−component of Eq (20) is obtained as follows:

$$uu_x + vu_y + \lambda_1(u^2 u_{xx} + v^2 u_{yy} + 2uvu_{xy}) = u_e(u_e)_x + vu_{yy} - \frac{\sigma}{\rho}B_0^2(u - u_e + \lambda_1 vu_y)$$

$$+ g\beta_T[(T - T_\infty) + \lambda_1\{uT_x + vT_y - u_x(T - T_\infty)\}], \qquad (21)$$

where we have used $\left[-\left(1 + \lambda_1 \frac{D}{Dt}\right)\nabla p\right]_x = u_e\frac{du_e}{dx} + \frac{\sigma}{\rho}B_0^2 u_e$.

Acknowledgments

Author Contributions

Conceptualization: Ammar Mushtaq, Meraj Mustafa, Tasawer Hayat, Ahmed Alsaedi.

Data curation: Ammar Mushtaq, Meraj Mustafa.

Formal analysis: Ammar Mushtaq, Meraj Mustafa.

Investigation: Ammar Mushtaq.

Methodology: Ammar Mushtaq, Meraj Mustafa, Tasawer Hayat, Ahmed Alsaedi.

Project administration: Meraj Mustafa.

Software: Meraj Mustafa.

Supervision: Meraj Mustafa, Tasawer Hayat, Ahmed Alsaedi.

Validation: Ammar Mushtaq, Meraj Mustafa.

Visualization: Ammar Mushtaq, Meraj Mustafa.

Writing – original draft: Ammar Mushtaq, Meraj Mustafa, Tasawer Hayat, Ahmed Alsaedi.

Writing – review & editing: Ammar Mushtaq, Meraj Mustafa, Tasawer Hayat, Ahmed Alsaedi.

References

1. Sadeghy K, Hajibeygi H, Taghavi SM (2006) Stagnation point flow of upper-convected Maxwell fluids. Int. J. Non-Linear Mech. 41: 1242–1247.

2. Kumari M, Nath G (2009) Steady mixed convection stagnation-point flow of upper convected Maxwell fluids with magnetic field. Int. J. Non-linear Mech. 44: 1048–1055.

3. Hayat T, Abbas Z, Sajid M (2009) MHD stagnation-point flow of an upper-convected Maxwell fluid over a stretching surface. Chaos Sol. & Fract. 39: 840–848.

4. Mukhopadhyay S (2012) Heat transfer analysis of the unsteady flow of a Maxwell fluid over a stretching surface in the presence of a heat source/sink. Chin. Phys. Lett. 29: https://doi.org/10.1088/0256-307X/29/5/054703

5. Motsa SS, Khan Y, Shateyi S (2012) A new numerical solution of Maxwell fluid over a shrinking sheet in the region of a stagnation point. Mathematic. Prob. Eng. 2012: Article ID 290615, http://dx.doi.org/10.1155/2012/290615.

6. Renardy M, Wang X (2012) Boundary layers for the upper convected Maxwell fluid. J. Non-Newtonian Fluid Mech. 189–190: 14–18.

7. Shateyi S (2013) A new numerical approach to MHD flow of a Maxwell fluid past a vertical stretching sheet in the presence of thermophoresis and chemical reaction. Bound. Val. Prob. 196: https://doi.org/10.1186/1687-2770-2013-196

8. Bhattacharyya K, Hayat T, Alsaedi A (2014) Dual solutions in boundary layer flow of Maxwell fluid over a porous shrinking sheet. Chinese Phys. B 23: Article ID 124701, https://doi.org/10.1088/1674-1056/23/12/124701.

9. Kumari M, Nath G (2014) Steady mixed convection flow of Maxwell fluid over an exponentially stretching vertical surface with magnetic field and viscous dissipation. Meccanica 49: 1263–1274.

10. Abbasbandy S, Naz R, Hayat T, Alsaedi A (2014). Numerical and analytical solutions for Falkner–Skan flow of MHD Maxwell fluid. Appl. Math. Comput. 242: 569–575.

11. Nandy SK (2015) Unsteady flow of Maxwell fluid in the presence of nanoparticles toward a permeable shrinking surface with Navier slip. J. Taiwan Inst. Chem. Eng. 52: 22–30.

12. Shafique Z, Mustafa M, Mushtaq A (2016) Boundary layer flow of Maxwell fluid in rotating frame with binary chemical reaction and activation energy. Resul. in Phys. 6: 627–633.

13. Bai Y, Liu X, Zhang Y, Zhang M (2016) Stagnation-point heat and mass transfer of MHD Maxwell nanofluids over a stretching surface in the presence of thermophoresis. J. Molec. Liq. 224: 1172–1180.

14. Khan N, Mahmood T, Sajid M, Hashmi MS (2016) Heat and mass transfer on MHD mixed convection axisymmetric chemically reactive flow of Maxwell fluid driven by exothermal and isothermal stretching disks. Int. J. Heat Mass Transf. 92: 1090–1105.

15. Mustafa M (2017) An analytical treatment for MHD mixed convection boundary layer flow of Oldroyd-fluid utilizing non-Fourier heat flux model. Int. J. Heat & Mass Transf. 113: 1012–1020.

16. Mustafa M, Hayat T, Alsaedi A (2017) Rotating flow of Oldroyd-B fluid over stretchable surface with Cattaneo-Christov heat flux: analytic solutions, Int. J. Numer. Meth. Heat & Fluid Flow, In press, https://doi.org/10.1108/HFF-08-2016-0323

17. Abdulhameed M, Vieru D, Roslan R (2017) Magnetohydrodynamic electroosmotic flow of Maxwell fluids with Caputo–Fabrizio derivatives through circular tubes. Comp. & Math. Appl., In press, https://doi.org/10.1016/j.camwa.2017.07.040.

18. Fourier JBJ (1822) Theorie Analytique Da La Chaleur. Paris (1822).

19. Cattaneo C (1948) Sulla conduzionedelcalore, AttiSemin. Mat. Fis. Univ. Modena Reggio Emilia 3: 83–101.

20. Christov CI (2009) On frame indifferent formulation of the Maxwell-Cattaneo model of finite speed heat conduction. Mech. Res. Commun. 36: 481–486.

21. Straughan B (2010) Thermal convection with the Cattaneo–Christov model, Int. J. Heat Mass Transf. 53: 95–98.

22. Tibullo V, Zampoli V (2011) A uniqueness result for the Cattaneo–Christov heat conduction model applied to incompressible fluids. Mech. Research Commun. 38: 77–79.

23. Haddad SAM (2014) Thermal instability in Brinkman porous media with Cattaneo–Christov heat flux. Int. J. Heat Mass Transf. 68: 659–668.

24. Han S, Zheng L, Li C, Zhang X (2014). Coupled flow and heat transfer in viscoelastic fluid with Cattaneo–Christov heat flux model. App. Math. Lett. 38: 87–93.

25. Mustafa M (2015) Cattaneo-Christov heat flux model for rotating flow and heat transfer of upper convected Maxwell fluid. AIP Advances 5: https://doi.org/10.1063/1.4917306

26. Khan JA, Mustafa M, Hayat T, Alsaedi A (2015). Numerical study of Cattaneo-Christov heat flux model for viscoelastic flow due to an exponentially stretching surface. PLoS ONE 10: https://doi.org/10.1371/journal.pone.0137363 PMID: 26325426

27. Hayat T, Qayyum S, Imtiaz M, Alsaedi A (2016) Three-dimensional rotating flow of Jeffrey fluid for Cattaneo-Christov heat flux model. AIP Advances 6: https://doi.org/10.1063/1.4942091

28. Mushtaq A, Abbasbandy S, Mustafa M, Hayat T, Alsaedi A (2016) Numerical solution for Sakiadis flow of upper-convected Maxwell fluid using Cattaneo-Christov heat flux model. AIP Advances 6: https://doi.org/10.1063/1.4940133

29. Salahuddin T, Malik MY, Hussain A, Bilal S, Awais M (2016) MHD flow of Cattanneo–Christov heat flux model for Williamson fluid over a stretching sheet with variable thickness: Using numerical approach. J. Magn. Magn. Mater. 401: 991–997.

30. Rubab K, Mustafa M (2016) Cattaneo-Christov heat flux model for MHD three-dimensional flow of Maxwell fluid over a stretching sheet. PLoS ONE 11: https://doi.org/10.1371/journal.pone.0153481 PMID: 27093542

31. Liu L, Zheng L, Liu F, Zhang X (2016) An improved heat conduction model with Riesz fractional Cattaneo–Christov flux. Int. J. Heat Mass Transf. 103: 1191–1197.

32. Abbasi FM, Shehzad SA (2016) Heat transfer analysis for three-dimensional flow of Maxwell fluid with temperature dependent thermal conductivity: Application of Cattaneo-Christov heat flux model. J. Mol. Liq. 220: 848–854.

33. Liu L, Zheng L, Liu F, Zhang X (2017) Heat conduction with fractional Cattaneo–Christov upper-convective derivative flux model. Int. J. Therm. Sci. 112: 421–426.

34. Mustafa M, Hayat T, Alsaedi A (2017) Rotating flow of Maxwell fluid with variable thermal conductivity: An application to non-Fourier heat flux theory. Int. J. Heat Mass Transf. 106: 142–148.

35. Hiemenz K (1911) Die Grenzschict neinem in den gleichformigen flussigkeitsstrom eingetauchten geraden Kreiszylinder. Dingl. Polytec. J. 326: 321–410.

36. Mahapatra TR, Nandy SK, Gupta AS (2009) Magnetohydrodynamic stagnation-point flow of a power-law fluid towards a stretching surface. Int. J. Non-Linear Mech. 44: 124–129.

37. Bhattacharyya K, Arif MG, Pramanik WA (2012) MHD boundary layer stagnation-point flow and mass transfer over a permeable shrinking sheet with suction/blowing and chemical reaction. Acta Technica 57: 1–15.

38. Bhattacharyya K, Mukhopadhyay S, Layek GC (2012) Reactive solute transfer in magnetohydrodynamic boundary layer stagnation-point flow over a stretching sheet with suction/blowing. Chem. Engg. Commun. 199: 368–383.

39. Bhattacharyya K (2013) Heat transfer in boundary layer stagnation-point flow towards a shrinking sheet with non-uniform heat flux. Chinese Phys. B 22: Article ID: 074705, https://doi.org/10.1088/1674-1056/22/7/074705.

40. Bhattacharyya K (2015) Reactive solute transfer in a stagnation-point flow over a shrinking sheet with a diffusive mass flux. J. Appl. Mech. Tech. Phys. 56: 464–470.

41. Patil PM, Roy S, Chamkha AJ (2010) Mixed convection flow over a vertical power law stretching sheet. Int. J. Numer. Meth. Heat & Fluid Flow 20: 445–458.

42. Mahmoud MAA, Waheed SE (2013) Mixed convection flow of a micropolar fluid past a vertical stretching surface in a thermally stratified porous medium with thermal radiation. J. Mech. 29: 461–470.

43. Gireesha BJ, Chamkha AJ, Manjunatha S, Bagewadi CS (2013) Mixed convective flow of a dusty fluid over a vertical stretching sheet with non-uniform heat source/sink and radiation. Int. J. Num. Meth. Heat & Fluid Flow 23: 598–612.

44. Ali FM, Nazar R, Arifin NM, Pop I (2014) Mixed convection stagnation-point flow on vertical stretching sheet with external magnetic field. Appl. Math. Mech.-Engl. Ed. 35: 155–166.

45. Hayat T, Qayyum S, Imtiaz M, Alsaedi A (2016) Comparative study of silver and copper water nanofluids with mixed convection and nonlinear thermal radiation. Int. J. Heat Mass Transf. 102: 723–732.

46. Mustafa M, Khan JA, Hayat T, Alsaedi A (2017) Buoyancy effects on the MHD nanofluid flow past a vertical surface with chemical reaction and activation energy. Int. J. Heat Mass Transf. 108: 1340–1346.

47. Turkyilmazoglu M (2017) Mixed convection flow of magnetohydrodynamic micropolar fluid due to a porous heated/cooled deformable plate: Exact solutions. Int. J. Heat Mass Transf. 106: 127–134.

48. Mohammadein (2010) Free convection through conducting non-Newtonian fluids over a thin axisymmetric body, Mecc. 45: 89–96.

49. Khan NA, Gul T, Islam S, Khan W (2017) Thermophoresis and thermal radiation with heat and mass transfer in a magnetohydrodynamic thin-film second-grade fluid of variable properties past a stretching sheet. The European Physical Journal Plus 132: https://doi.org/10.1140/epjp/i2017-11277-3

50. Gul T, Khan AS, Islam S, Alqahtani AM, Khan I, Alshomrani AS, Alzahrani AK, Muradullah (2017) Heat transferinvestigation of the unsteady thin film flow of Williamson fluid past an inclined and oscillating moving plate, Applied Sci. 7: https://doi.org/10.3390/app7040369

51. Ali L, Islam S, Gul T, Alshomrani A, Khan I, Aurangzeb K (2017), Magnetohydrodynamics thin film fluid flow under the effect of thermophoresis and variable fluid properties, AIChE Journal: https://doi.org/10.1002/aic.15794

52. Abel MS, Tawade JV, Nandeppanavar MM (2012) MHD flow and heat transfer for the upper convected Maxwell fluid over a stretching sheet. Mecc. 47: 385–93.

53. Megahed AM (2012) Variable fluid properties and variable heat flux effects on the flow and heat transfer in a non-Newtonian Maxwell fluid over an unsteady stretching sheet with slip velocity. Chin. Phys. B 22: Article ID 094701, https://doi.org/10.1088/1674-1056/22/9/094701